ACCEPTED MANUSCRIPT
DOI of the published work: https://doi.org/10.1016/j.jobe.2022.104805
Journal of Building Engineering, Volume 56, 15 September 2022, 104805

Mechanical characterization and elastic stiffness degradation of unstabilized rammed earth

Luisa María Gil-Martín[a], Manuel Alejandro Fernández-Ruiz[b,*], Enrique Hernández-Montes[c]

[a] Department of Structural Mechanics, University of Granada (UGR). Campus Universitario de Fuentenueva s/n. 18072 Granada, Spain. mlgil@ugr.es.

[b] Department of Industrial and Civil Engineering, University of Cádiz (UCA). Campus Bahía de Algeciras, Avda. Ramón Puyol, s/n. 11201 Algeciras (Cádiz), Spain. manuelalejandro.fernandez@uca.es.
*Corresponding author.

[c] Department of Structural Mechanics, University of Granada (UGR). Campus Universitario de Fuentenueva s/n. 18072 Granada, Spain. emontes@ugr.es.

Abstract

Rammed earth is attracting renewed interest due to its sustainability. In this work, a mechanical characterization of unstabilized rammed earth is presented. Compressive strength, Young's modulus, and Poisson's ratio were determined, with the first of these being the most representative mechanical property of rammed earth. Stress – strain curves were obtained from uniaxial compression tests. Creep is of great importance in the long-term assessment of historical buildings and in the design of new ones. Samples of rammed earth were subjected to a constant load for 15 days to study their creep behavior. In order to simulate the long-term behavior of the material, different rheological models were fitted to the experimental results. The instantaneous deformation of rammed earth samples caused by a sudden additional load (maintaining a previous service load level) was also studied. This is the first time that this

phenomenon, called elastic stiffness degradation, has been studied for rammed earth material.

Keywords: Rammed earth; Creep; Compressive strength; Mechanical properties; Instantaneous response after creep.

1. Introduction

Earth is considered to be one of the most important historical construction materials. There is evidence of mud brick buildings constructed ten thousand years ago in the Middle East and North Africa [1]. Earth construction is present in many areas of the world, especially in warm and arid climate zones. This is due to its worldwide availability at little or no cost and its mechanical characteristics [1,2].

There are several earth construction techniques. Rammed Earth (RE) is an ancient building technique that consists of dynamically compacting layers of moist soil between removable formworks to create monolithic walls with a thickness of 30 cm to 60 cm [3,4]. The layers of about 7.5 to 15 cm thick [5,6] are compacted by the use of a rammer (manual or pneumatic), and the process is repeated until the wall is completed. The compaction is usually carried out at the optimum moisture content of the soil, which corresponds to the highest dry density for a given compaction energy [7,8]. Standard [9] or modified [10] Proctor tests can be used to determine the optimum moisture content.

In the traditional rammed earth construction (called unstabilized rammed earth), the only binder is clay. In the case of stabilized rammed earth, other binders such as cement, lime or coal ash are added in order to increase its durability and mechanical properties [11–13]. However, the use of these binders increases the construction cost and its environmental impact.

RE was used in the construction of residential and heritage buildings from 2300 – 1810 BC [14]. More than 10% of the assets declared as Cultural Heritage (CH) of Humanity by UNESCO are structures made of RE [15]. The Alhambra in Granada [16] and the Great Wall of China are examples of these types of structures. The characterization of the building materials is one of the biggest challenges at CH sites in order to improve its resilience to cope with climate change and extreme events.

In the current context of sustainable development in the construction sector, RE is attracting the attention of the scientific community because it offers great environmental advantages in comparison with other construction materials. RE has a low level of embodied energy because soil is a locally sourced and unprocessed material [17]. In addition, during RE constructions there is no need for toxic or pollutant materials, only wooden formworks and rammers are needed. Finally, the thickness of RE walls and the low thermal conductivity of soil act as a form of natural moisture buffering for indoor environments [18–20].

There are several scientific works related to RE in the literature. The durability and the influence of moisture on the mechanical characteristics of RE were studied in [21,22] and [23,24], respectively. Numerous works about the mechanical properties of RE, such as unconfined compressive strength [3,8,25,26], Young's modulus [23,25,27–29], Poisson's ratio [27,30], tensile strength [27,31], and shear strength [30,32] can be found in the literature. The thermal [33–35], hygrothermal [18,36], and acoustic [37] properties of RE have been also studied. However, a very limited number of scientific works about the creep behavior of unaltered RE can be found. In Bui and Morel [6,38], RE walls exposed for 22 years to natural weathering were tested (after altering the mass) and the creep phenomenon was studied. In addition, the number of scientific works about the elastic stiffness degradation of RE is also very low. In [39], the

stiffness degradation of unstabilized RE due to cyclic loading was analyzed. It was concluded that the stiffness was sensitive to the stress level (a higher degradation occurred with an increase of the stress level). The deterioration of RE constructions is one of the biggest challenges in conservation. Aspects such as the structural response of RE material subjected to a sudden load such as an earthquake or to cyclic loading must be considered for the structural assessment of RE constructions.

In this work, the mechanical properties of RE are studied. Basic mechanical properties such as unconfined compressive strength, Young's modulus, and Poisson's ratio were obtained from their corresponding tests. The stress-strain relationships obtained from the compression tests were also computed. The creep behavior of RE was determined from cylindrical samples subjected to a constant stress for 15 days. At the end of the creep tests, all the specimens were subjected to an additional load in order to estimate the instantaneous elastic response of RE under a sudden load in order to get information for a seismic analysis of RE structures. In doing so, this phenomenon, denominated elastic stiffness degradation, is first presented for RE. Several rheological models were fitted to the experimental results of RE.

2. Experimental methodology

2.1. Materials used

The earth material used in this work was taken from an existing quarry located 45 km from the city of Granada (Spain). Particles larger than 20 mm were removed from the soil by sieving. The Particle Size Distribution (PSD) of this soil was carried out in accordance with the ISO 17892-4:2016 Standard [40] by sieving (for elements > 0.063 mm) and by using the laser diffraction method (for elements < 0.063 mm). According to some studies [41,42], the PSD of the soil used should not be considered as a

discriminatory parameter for studying soil suitability for RE construction. However, a heterogeneous particle size distribution (including both fine and coarse particles) is generally recommended for RE construction [3,43,44]. Figure 1 shows the PSD of the soil employed in this work.

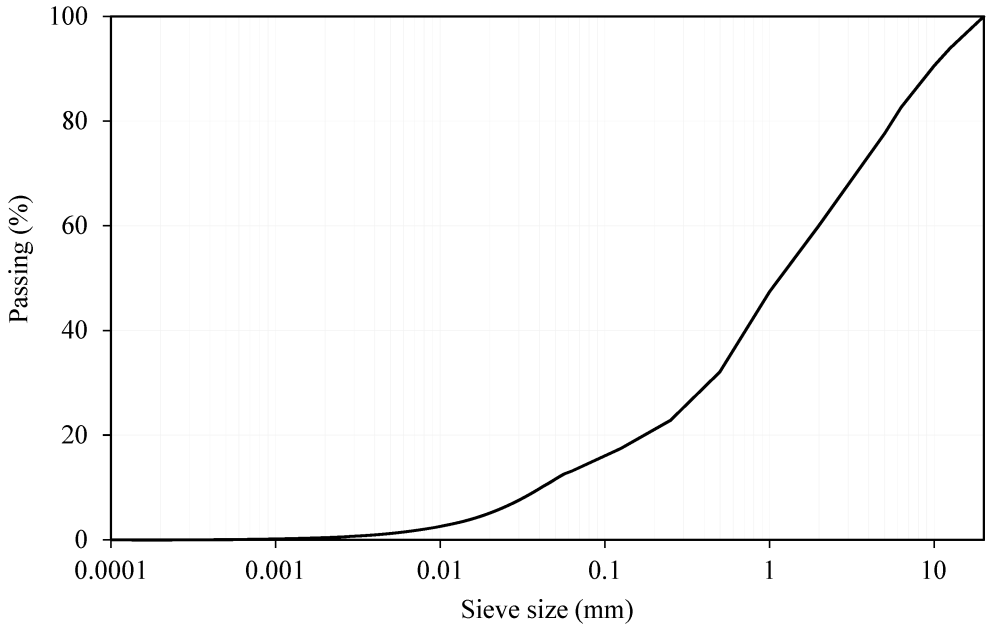

Figure 1. Particle size distribution

According to the PSD shown in Figure 1, it can be said that the soil employed in this work is a silty sand with a maximum aggregate size of 20 mm, which is suitable for RE construction without stabilization (but lacks of cohesion erodes easily and sometimes fine soils should be added) [44]. The clay mineralogy, as determined by X-Ray Diffraction (XRD), was predominantly illite with presence of smectite, and chlorite.

A key aspect of the soil used in RE construction is its moisture content [24,43]. A value of moisture content equal to the optimum moisture content ± 1 – 2% is recommended by Walker et al. [43]. In order to determine the optimum moisture content, the Standard Proctor test procedure, in accordance with the Spanish UNE 103-500-94 [9] Standard, was used. A range of water content (7 – 12%) was selected to obtain the maximum dry density. Figure 2 shows that the optimum moisture content for RE manufacturing was

8% by mass. This result is in line with the values of optimum moisture content obtained in other research works present in the literature, which ranges between 8 – 12% by weight [5,23,29,30].

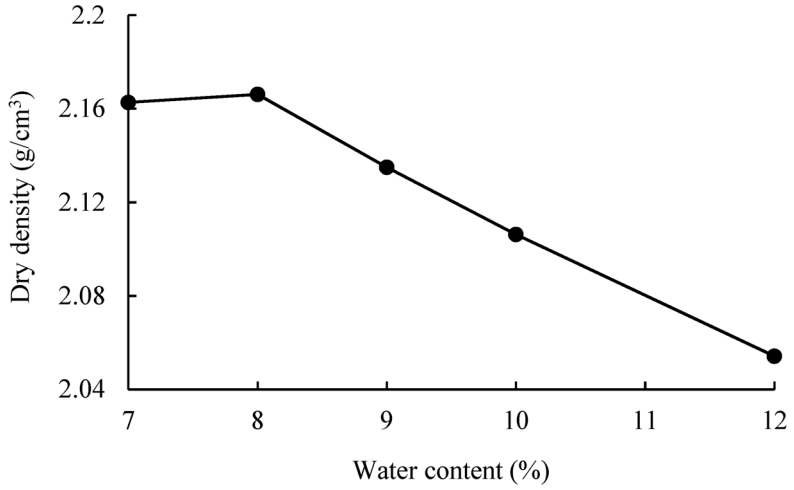

Figure 2. Results of the Standard Proctor test

2.2. RE samples manufacturing

The earth material was hand-mixed with the optimum moisture content (8% by mass). A cylindrical mold (15 cm diameter, 30 cm height) was used to prepare the samples. Consequently, the resulting RE samples had an aspect ratio of 2 (according to [45], it is important to avoid smaller aspect ratios). The maximum aggregate size of the soil employed in this work is 20 mm. In historical RE constructions a wide range of RE material particle size can be observed (the maximum aggregate size can reach 60 mm or more [4]). Mechanical parameters such as the unconfined compressive strength can be affected by the high maximum aggregate size with respect to the specimen size [4]. According to [46,47], in this campaign the diameter of the samples is higher than 3.5 times the maximum aggregate size of the soil employed. The moist soil was poured into the mold and compacted in 6 layers with 2 kg of material for each one. Each layer was compacted manually with standard Proctor rammer. The objective of this manufacturing

strategy is to obtain a RE sample as similar as possible to *in situ* material. After the compaction process, the RE samples were removed from the molds.

The samples were left to dry for 4 months in normal atmospheric conditions. They were considered *"air-dry"* when the moisture content remained constant, which occurred, approximately, on the 25th day. For example, this *"air-dry"* state is the ambient condition of *in situ* RE walls in service [8]. Finally, the bottom and top surfaces of the RE samples were capped with a mortar in order to provide a smooth flat surface. This was done in order to achieve a uniform distribution of stresses during testing.

2.3. Unconfined compressive strength

Twelve samples were tested under uniaxial compression to obtain their Unconfined Compressive Strength (UCS). The RE specimens were tested between two hardened steel plates using a hydraulic actuator with a capacity of 1000 kN. During the tests, the load was increased monotonically in load control at a rate of 0.05 kN/s.

Due to the crumbly nature of the RE specimens tested, the use of contact measurement sensors without affecting neither the sample integrity nor the load response of the unstabilized rammed earth samples is difficult. Given that the global average strains are the objective of the study, a gross estimation of the specimen strains, i.e. based on the plate-to-plate displacement, is done, which is appropriate for structural purposes. To study local strains or to do a more detailed study of the sample strains, optical techniques to track markers on the surface of the samples during loading regimens, high-speed cameras, and video dimensional analyzers, among others methods would be more appropriate [27,29].

In order to detect possible oscillations of the loading plate and to properly measure the post-peak strain of the specimens, two diametrically opposed LVDTs with a range of 100 mm were set during the compression test (see Figure 3). The longitudinal

displacement during the compression tests was measured using the two LVDTs. Thus, the longitudinal strain was determined based on the average reading of these two LVDTs considering the initial length of the sample as in [8,23,25]. In addition, two other LVDTs with a range of 10 mm were used to measure the transversal deformation. Stress – strain curves were obtained from each compression test. Figure 3 shows the configuration of the UCS test carried out.

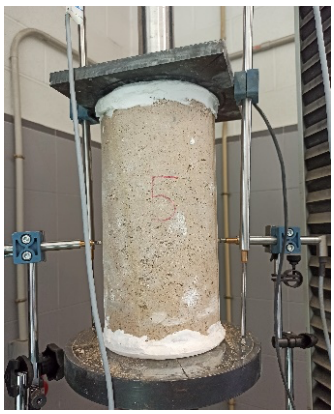

Figure 3. Unconfined compressive strength test of rammed earth

2.4. Young's modulus and Poisson's ratio

Young's modulus of RE (E_{RE}) was obtained from the stress – strain curve registered during the unconfined compressive strength tests. Poisson's ratio was also obtained from the compression tests by measuring vertical and lateral displacements with LVDT sensors (see Figure 3).

2.5. Creep test

A uniaxial compression test at constant load was carried out for six samples in order to study the creep behavior of RE. The load was introduced through a lever onto each RE sample. This mechanism allowed the application of a constant load (the self-weight of the steel beam) during the creep test (see Figure 4.a). The constant load value used in all the creep tests was determined based on previous compression tests (the maintained stress was set around 15% of the average compressive strength of RE). A load cell was

used to measure the load applied to the specimen. The constant compressive stress corresponding to the applied load was approximately 0.1 MPa and it was maintained for 15 days, at which time the deformation was proved to be stabilized. The longitudinal strain of the RE sample was determined based on the readings of a LVDT with a range of 10 mm (see Figure 4.b) considering the total length of the sample.

(a) (b)

Figure 4. Configuration of the creep tests (a) and detail of the test (b)

2.6. Immediate response of RE samples after creep tests: Elastic Stiffness Degradation

The study of the structural response of RE material subjected to a sudden load such as an earthquake or an impact in service conditions is very important for the structural assessment of RE constructions.

In order to study this effect, an instantaneous additional compressive load was applied to all the specimens at the end of the creep test (keeping the sustained load applied, see Figure 5). The new load was applied to the samples by using a concrete cube as indicated in Figure 5. By doing so, an additional stress of around 2% of the average compressive strength of RE was applied to the specimens. The stress – strain curve associated to the application of this instantaneous load was obtained based on the values recorded using the same set-up that for the creep test (see Figure 4.b). The post-creep Young's modulus of RE (called E'_{RE}) was obtained as the average ratio between the

stress increment and its corresponding strain increment during the application of the additional load.

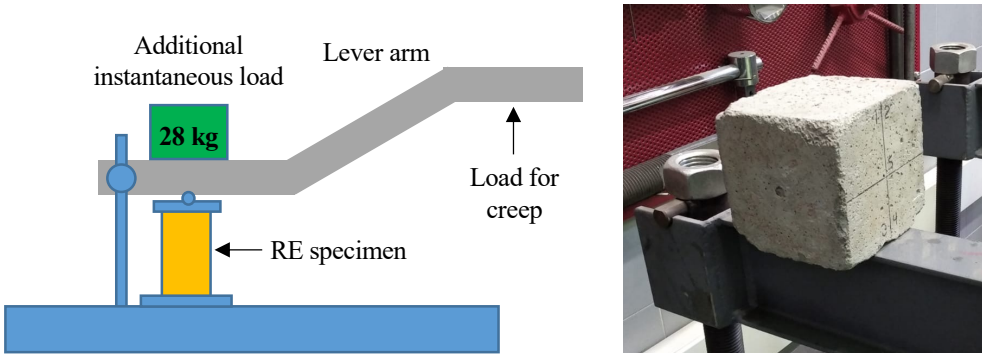

(a) (b)

Figure 5. Stiffness degradation test for RE (a) and detail of the additional instantaneous load introduced at the end of the creep tests (b)

3. Results and discussion of the experimental campaign

3.1. Unconfined compression strength and stress-strain curves

The average Unconfined Compressive Strength (UCS) was 0.74 ± 0.1 MPa. There are several works about the UCS of RE in the literature. Due to the wide range of parameters that affects UCS (sample size and shape, testing procedure, compaction, PSD of the soil material, maximum aggregate size, etc.) there is a significant dispersion in the results. For example, Bui et al. [8] indicated that the UCS obtained for small samples was higher than that obtained for the bigger ones. In addition, samples with a low slenderness ratio (for example cubic specimens) do not give direct results. That is the reason why Hall and Djerbib [3] used a correction factor of 0.7 for their compressive strength results in their study. The shape of the sample also affects the UCS of RE. Several studies present in literature such as [8,25,29] have reported differences between the UCS of prismatic and cylindrical samples. Cylindrical specimens can be compacted in an easier way without a significant friction with the formwork than prismatic samples, resulting in a better mechanical behavior in the case of the first ones. Besides,

the load distribution pattern is different, affecting the resultant value of UCS. Due to the wide range of parameters that affect UCS it is difficult to determine a clear relationship between them and UCS. However, based on works present in literature [3,8,23,25,48], the UCS of RE can be established within the range 0.7 – 2.5 MPa. The average UCS obtained in this work is in the lowest part of this range. This can be due to the dimensions of the samples (the cylindrical samples tested in this work had greater dimensions than the cylindrical samples tested in [23,25,48]), resulting in a lower value of UCS according to [8] or to the PSD of the soil employed.

Stress – strain ($\sigma - \varepsilon$) curves were calculated as $\sigma = N/A$ (where N is the axial load and A is the original cross-sectional area of the RE sample), and $\varepsilon = \Delta l/l$ (where Δl is the axial deformation relative to the initial length of the RE sample, and l is the initial length of the sample). All the RE samples tested showed a similar $\sigma - \varepsilon$ curve. The average $\sigma - \varepsilon$ curve of RE is shown in Figure 6.

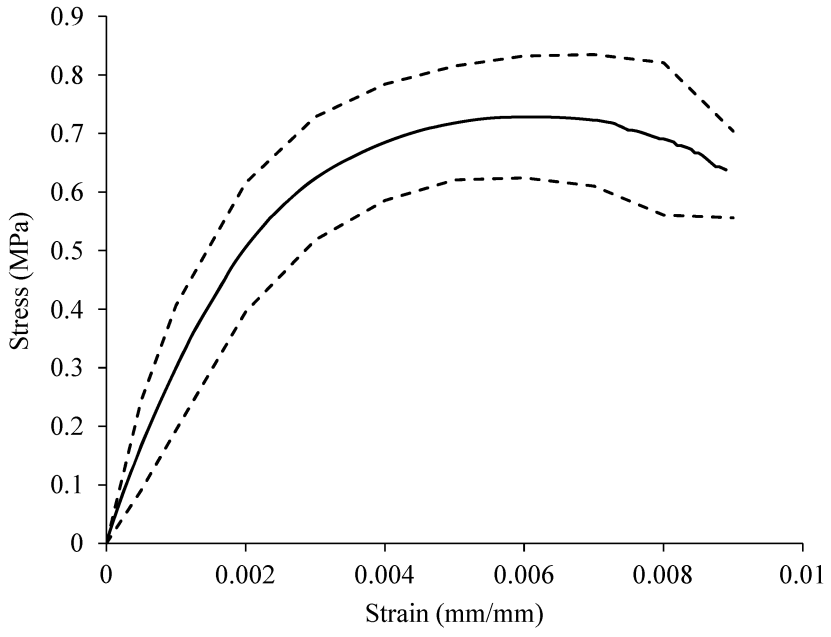

Figure 6. Average stress-strain curves of all the RE samples tested (black curves) ± the standard deviation (dashed black curves)

The ultimate strain recorded is in line with the results shown in [6] (which was 0.008 ± 0.001).

3.2. Elastic properties of RE (Young's modulus and Poisson's ratio)

Young's modulus E_{RE} = 330.11 ± 133.40 MPa was calculated using the following equation [23]:

$$E_{RE} = \frac{S_2 - S_1}{\varepsilon - 0.00005} \quad (1)$$

In Eq. (1) E_{RE} is the Young's modulus of RE, S_2 is the stress corresponding to 40% of UCS, S_1 is the stress corresponding to a longitudinal strain of 0.00005 and ε is the longitudinal strain produced by the stress S_2. As in the case of UCS, there is a significant dispersion in the values of the Young modulus of RE reported in the literature, ranging from about 60 to 1000 MPa [23,25,27–29]. Such dispersion is related to the sample manufacturing (soil employed, moisture content and sample size and shape) [25,27]. In addition, the testing procedure and the deformation measurement set-up affect the elastic modulus of RE. Alós Shepherd et al. [49] concluded that, in the case of plastic concrete, the elastic modulus determined following geotechnical standards (that commonly use the total platen displacement) is lower than the one obtained from concrete testing standards (that measure the deformation of the sample using strain gauges or similar). In this work, the strain has been computed considering the total platen displacement as in [8,23,25] and the corresponding Young's modulus of RE obtained in these works are in the range 90 to 350 MPa. On the other hand, in Bui et al. [27] extensometers were used to measure the strain at the central part of the specimen and in El-Nabouch et al. [29] the strain was measured using digital image correlation. The value of the Young's modulus of RE obtained in both studies was 500 ± 40 MPa and 763 ± 54 MPa. It can be seen that the conclusion presented in Alós

Shepherd et al. [49] is fulfilled in this specific case for RE; however, more research is needed to confirm it.

The Poisson's ratio of RE samples was $\nu = 0.21 \pm 0.03$. Unlike the Young's modulus, only a few works about the Poisson's ratio of RE are present in the literature. Bui et al. [27] reported a value of $\nu = 0.22 \pm 0.01$ and Miccoli et al. [30] a value of $\nu = 0.27 \pm 0.04$. The Poisson's ratio obtained in this work is in line with the values noted in the literature.

3.3. Creep

Figure 7.a and 7.b show the average total (ε_{tot}) and creep (ε_{cc}) strain respectively for all the RE samples tested. The time-dependent strain (creep strain) was obtained by subtracting the instantaneous elastic strain from the total axial strain.

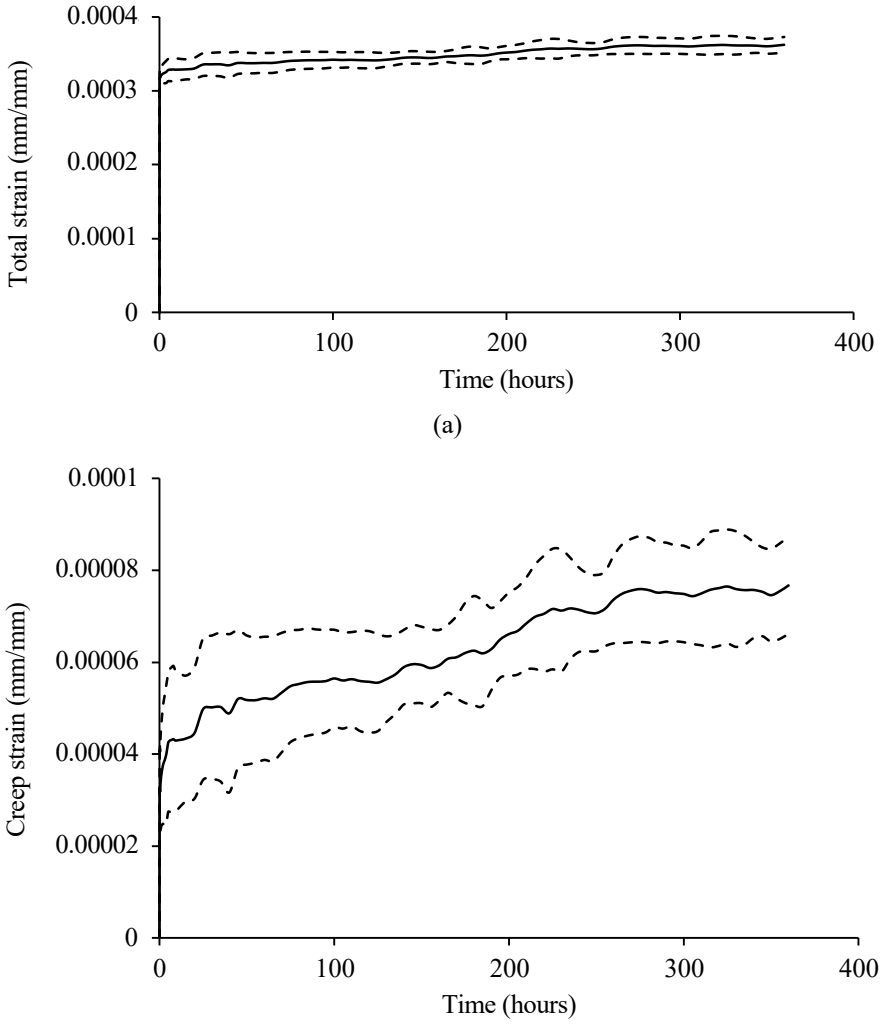

Figure 7. Average total strain (a) and creep strain (b) in time of all the RE samples tested (continuous black curve) ± the standard deviation (dashed black curves)

In Bui and Morel [6,38], RE walls were exposed to natural weathering and subjected to its own weight for 22 years. There was not any experimental set-up in order to measure the deformation or the stress in any part of the RE wall. The Young's modulus of the new specimens (made with the same material than the RE walls) was 2.7 times greater than the ones of the old RE walls. Omitting the possible problem of representativeness of the new specimens, Bui and Morel obtained a creep coefficient of 1.7 for RE. Bui and Morel [6,38] also indicated that the creep due to the maintained load was negligible because the stress level was low; however, the creep due to weathering could take place.

For concrete, following Eurocode 2 [50], the creep deformation at time t due to a constant compressive stress σ_0 applied at the concrete age t_0 is given by the following expression:

$$\varepsilon_{cc}(t,t_0) = \varphi(t,t_0)\frac{\sigma_0}{E_{RE}} \tag{2}$$

From the experimental campaign, the creep strain at t = 15 days is known (see Figure 7.b), σ_0 = 0.1 MPa and E_{RE} = 330.11 MPa; consequently, and according to Eq. (2), φ = 0.25 at 15 days for RE.

Different rheological models have been considered in order to estimate the long-term creep behavior of RE. The Burgers model [51] is constructed with two Hooke springs and two Newton dashpots (see Figure 8.a). The Kelvin model [52] consists of two Hooke springs and one Newton dashpot (see Figure 8.b). Finally, the fractional Maxwell model [53] is constructed with one Hooke spring and one Scott Blair dashpot (see Figure 8.c). The total strain of the rheological models shown in Figure 8.a, b and c are indicated in Eqs. (3), (4) and (5), respectively.

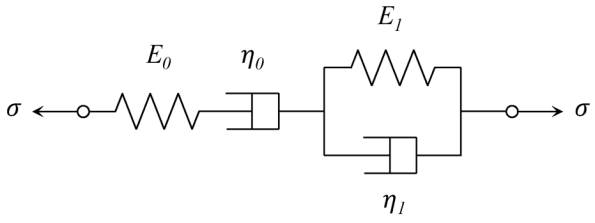

(a)

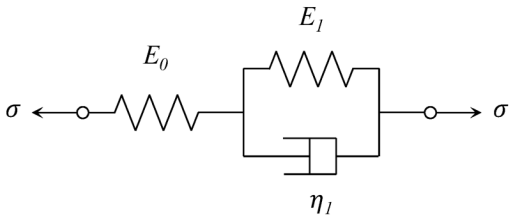

(b)

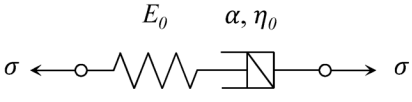

(c)

Figure 8. Burgers (a), Kelvin (b), and fractional Maxwell (c) rheological models.

$$\varepsilon(t) = \sigma_0 \left(\frac{1}{E_0} + \frac{1}{E_1}\left(1 - e^{\left(-\frac{E_1}{\eta_1}t\right)}\right) + \frac{t}{\eta_0} \right) \tag{3}$$

$$\varepsilon(t) = \sigma_0 \left(\frac{1}{E_0} + \frac{1}{E_1}\left(1 - e^{\left(-\frac{E_1}{\eta_1}t\right)}\right) \right) \tag{4}$$

$$\varepsilon(t) = \sigma_0 \left(\frac{1}{E_0} + \frac{1}{\eta_0^{\alpha}} \frac{t^{\alpha}}{\Gamma(1+\alpha)} \right) \tag{5}$$

In Eq. (5), Γ is the Gamma function (see Eq. (6)).

$$\Gamma(z) = \int_0^{\infty} t^{z-1} e^{-t} dt \tag{6}$$

The rheological models shown in Figure 8 have been adapted to the experimental creep results. The total strain ε corresponding to a given stress σ_0 can be expressed as the sum of the elastic strain ε_e (which is time independent) and the time-dependent strain ε_t. Eqs. (3), (4) and (5), show that the elastic strain is σ_0/E_0, as a result of Hooke's law. On the other hand, in the experimental creep results, the elastic strain has been removed. For this reason, in all the rheological models shown in Figure 8, the Hooke spring with E_0 was not considered when fitting the experimental data to these models. A nonlinear least squares fitting was carried out based on the expressions shown in Eqs. (3), (4), and (5) and the experimental creep curve. The parameters of the rheological models, the goodness of fit R^2, and the Mean Squared Error (MSE) corresponding to the average experimental creep curve shown in Figure 9 are shown in Table 1.

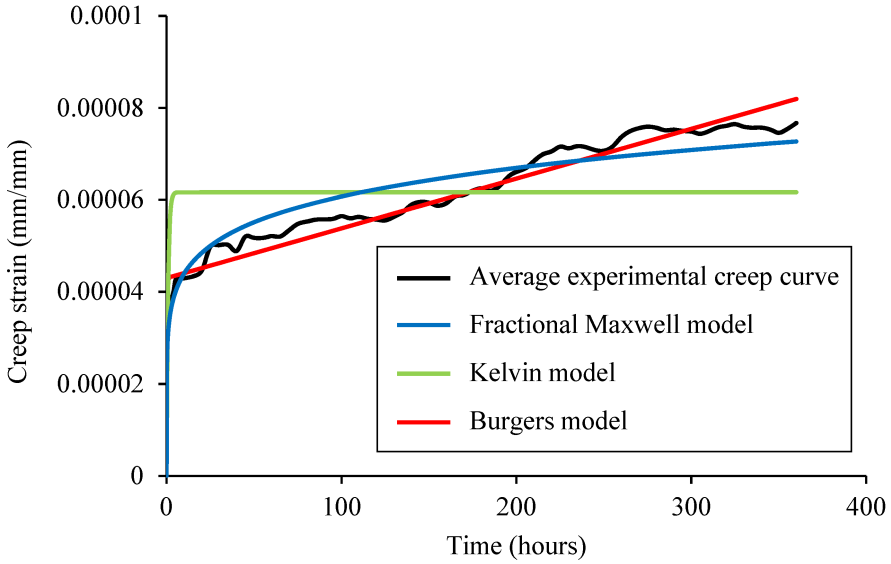

Figure 9. Fitting average experimental creep curve to three rheological models

Table 1. Fitting of creep results with the studied rheological models together with the coefficient of determination R^2 and the Mean Squared Error (MSE)

Model	Parameters	R^2	MSE
Burgers (Eq. (2))	$\eta_0 = 3.329\times10^6$ GPa·s	0.997	$1.21093*10^{-11}$
	$E_1 = 2.326$ GPa		
	$\eta_1 = 1.846\times10^3$ GPa·s		
Kelvin (Eq. (3))	$E_1 = 1.622$ GPa	0.963	$1.30631*10^{-10}$
	$\eta_1 = 4.834\times10^3$ GPa·s		
Fractional Maxwell (Eq. (4))	$\eta_0 = 10.577$ GPa·s$^\alpha$	0.995	$1.61064*10^{-11}$
	$\alpha = 0.140$		

Figure 9 shows the three rheological models considered in this work and the average experimental creep curve. Although a high value of R^2 has been obtained for all the rheological models considered, the fractional Maxwell model is the one which best agrees with the experimental creep curve over the range of time considered in comparison with the Burgers and Kelvin model. The MSE of Burgers and fractional Maxwell models are similar and lower than the one corresponding to the Kelvin model. The results in Figure 9 show that the Burgers model provides a better fit to the experimental results than the Kelvin model (which is reflected in the corresponding values of R^2 and MSE). This is because the Burgers model is a more complex

rheological model than the Kelvin one (see Figure 8), which is the simplest viscoelastic model, and so it may have some limitations when describing creep.

3.4. Elastic Stiffness Degradation of RE

The post-creep Young's modulus of RE was E'_{RE} = 264.7 ± 65.6 MPa. Figure 10 shows an example of the load-time graph record corresponding to the application of an instantaneous additional load in a RE sample after the creep test (keeping the maintained load, see Figure 5). The load record shown in Figure 10 corresponds only to the additional load. The value of E'_{RE} was computed as the average value of the increment of stress ($\Delta\sigma$) divided by the increment of strain ($\Delta\varepsilon$) associated at the application of the instantaneous additional load.

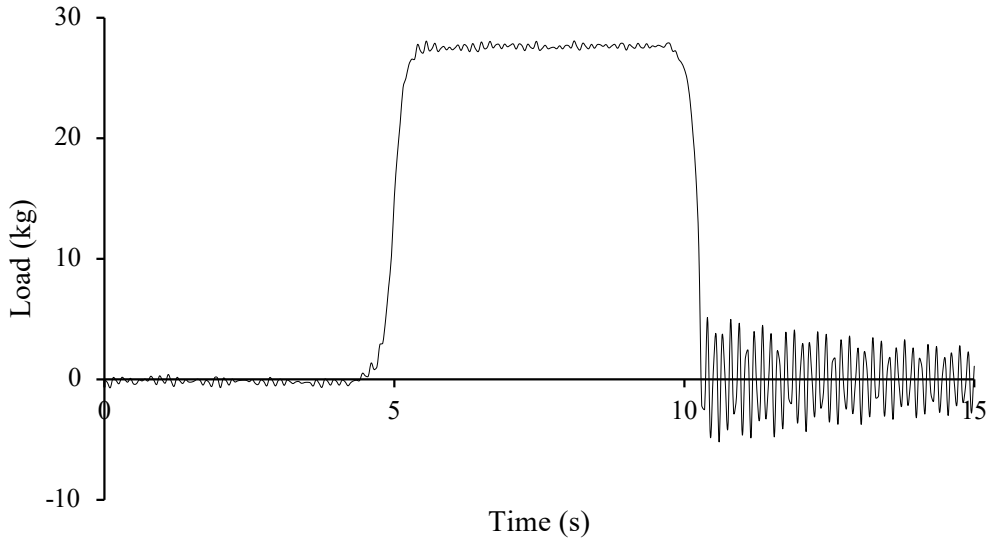

Figure 10. Example of the application of an instantaneous additional load in a RE sample after the creep test (keeping the maintained load which caused creep)

It is known that structural stiffness plays a significant role in the design given its influence in the response of the structure in terms such as the natural vibration period or the displacements [54]. At the material level, stiffness also is a good candidate parameter to be evaluated. Usually this parameter is obtained as the slope of the load–displacement hysteretic loops during cyclic tests, mainly in the context of fatigue and fracture behaviours (which are out of the scope of this work). In some materials the

stiffness degradation is just the consequence of cracks propagation and/or yielding [55]. On the contrary, in materials as concrete, the stiffness degradation depends on the level of strains [56].

A stiffness degradation effect can be observed if the values of E_{RE} and E'_{RE} are compared. This stiffness degradation was measured just at the end of the creep test so the influence of the loading time on the RE stiffness has not been considered here. Results show that a RE specimen subjected to dead loads will suffer a higher instantaneous deformation against a sudden load than a non-preloaded specimen. So, the total strain must be computed as in Eq. (7). This degradation effect can be particularly important in the case of a seismic evaluation of RE heritage structures, in which the current elastic modulus of the RE material must be considered. In Eq. (7) $\varphi(t, t_0)$ is the creep coefficient.

$$\varepsilon_{tot}(t) = \frac{\sigma_0}{E_{RE}} + \varphi(t,t_0)\frac{\sigma_0}{E_{RE}} + \frac{\Delta\sigma_t}{E'_{RE}} \quad (7)$$

4. Conclusions

In this work, the mechanical properties and the creep behavior of RE are studied. Cylindrical specimens (15 cm diameter, 30 cm height) were prepared, and the compressive strength, Young's modulus and Poisson's ratio were evaluated.

New experimental results for the creep behavior of RE has been presented. The modulus of elasticity before and after creep are evaluated. Based on the results obtained in this research, the following conclusions can be drawn:

1. The average unconfined compressive strength, Young's modulus and Poisson's ratio of the RE studied are 0.74 ± 0.1 MPa, 330.11 ± 133.40 MPa, and 0.21 ± 0.03, respectively.

2. A uniaxial compression test at constant load was carried out in order to study the creep behavior of RE. The compressive stress during the creep test was approximately a 15% of the average compressive strength of RE. Different rheological models (Burgers, Kelvin and fractional Maxwell models) have been fitted to the experimental creep results. The fractional Maxwell model showed the best fit to the experimental results over the full range of time. A creep coefficient of 0.25 has been computed at the end of the creep tests (15 days).
3. One of the biggest challenges in conservation of cultural heritage constructions is their structural assessment. To this end, it is essential the study of the deterioration of the mechanical properties due to extreme events and the long-term response of heritage building materials such as RE. An additional load was introduced at the end of the creep tests (keeping the sustained load applied) in order to evaluate instantaneous response of the specimen. The Young's modulus after creep tests was calculated as the ratio between increments of stress and strains: E'_{RE} = 264.7 ± 65.6 MPa. A stiffness degradation effect can be observed if the values of E_{RE} and E'_{RE} are compared. Consequently, RE specimens subjected to constant loads in time suffer a bigger instantaneous deformation against sudden applied loads than non-preloaded specimens. This phenomenon, denominated elastic stiffness degradation, is of great importance in seismic analysis.

Acknowledgements

This work is part of the HYPERION project (https://www.hyperion-project.eu/). HYPERION has received funding from the European Union Framework Programme for Research and Innovation (Horizon 2020) under grant agreement no. 821054. The

content of this publication is the sole responsibility of UGR and does not necessarily reflect the opinion of the European Union. The authors would like to gratefully acknowledge to Dr. Lourdes Jalón of the University of Granada for her help during the RE samples manufacturing. The authors would also like to thank Prof. Cultrone of the University of Granada for the analysis of the clay mineralogy by the XRD technique. Their support is gratefully acknowledged.

References:

[1] H. Niroumand, M.F.M. Zain, M. Jamil, S. Niroumand, Earth Architecture from Ancient until Today, Procedia - Soc. Behav. Sci. 89 (2013) 222–225. doi:10.1016/j.sbspro.2013.08.838.

[2] G. Minke, Building with Earth, Berlin, Boston: Birkhäuser., 2013. doi:https://doi.org/10.1515/9783034612623.

[3] M. Hall, Y. Djerbib, Rammed earth sample production: Context, recommendations and consistency, Constr. Build. Mater. 18 (2004) 281–286. doi:10.1016/j.conbuildmat.2003.11.001.

[4] J.J. Martín-del-Rio, J. Canivell, M. Torres-González, E.J. Mascort-Albea, R. Romero-Hernández, J.M. Alducin-Ochoa, F.J. Alejandre-Sánchez, Analysis of the materials and state of conservation of the medieval rammed earth walls of Seville (Spain), J. Build. Eng. 44 (2021) 103381. doi:https://doi.org/10.1016/j.jobe.2021.103381.

[5] Q.B. Bui, J.C. Morel, Assessing the anisotropy of rammed earth, Constr. Build. Mater. 23 (2009) 3005–3011. doi:10.1016/j.conbuildmat.2009.04.011.

[6] Q.B. Bui, J.C. Morel, First exploratory study on the ageing of rammed earth material, Materials (Basel). 8 (2015) 1–15. doi:10.3390/ma8010001.

[7] ASTM, D653-14 Standard Terminology Relating to Soil, Rock, and Contained Fluids, 2014. doi:https://doi.org/10.1520/D0653-11.2.

[8] Q.B. Bui, J.C. Morel, S. Hans, N. Meunier, Compression behaviour of non-industrial materials in civil engineering by three scale experiments: The case of rammed earth, Mater. Struct. Constr. 42 (2009) 1101–1116. doi:10.1617/s11527-008-9446-y.

[9] UNE_103-500-94, Ensayo de Compactación Proctor Normal, 1994.

[10] UNE_103-501-94, Ensayo de compactación Proctor modificado, in: 1994.

[11] B.V.V. Reddy, R.S. Bhanupratap Rathod, Influence of interlayer shear studs on the behaviour of cement stabilised rammed earth under compression, tension and shear, J. Build. Eng. 49 (2022) 104096. doi:https://doi.org/10.1016/j.jobe.2022.104096.

[12] G.S. Pavana, S.N. Ullas, K.S. Nanjunda Rao, Shear behavior of cement stabilized rammed earth assemblages, J. Build. Eng. 27 (2020) 100966. doi:https://doi.org/10.1016/j.jobe.2019.100966.

[13] Saranya Raj S., A.K. Sharma, K.B. Anand, Performance appraisal of coal ash stabilized rammed earth, J. Build. Eng. 18 (2018) 51–57. doi:https://doi.org/10.1016/j.jobe.2018.03.001.

[14] P.A. Jaquin, C.E. Augarde, C.M. Gerrard, Chronological description of the spatial development of rammed Earth techniques, Int. J. Archit. Herit. 2 (2008) 377–400. doi:10.1080/15583050801958826.

[15] D. Grandeau, L. Delboy, World heritage inventory of earthen architecture, Villefontaine, CRAterre-ENSAG, 2012.

[16] K. Elert, F. Jroundi, C. Benavides-Reyes, E. Correa Gómez, D. Gulotta, C. Rodríguez Navarro, Consolidation of clay-rich earthen building materials: A

441 comparative study at the Alhambra fortress (Spain), J. Build. Eng. 50 (2022)
442 104081. doi:https://doi.org/10.1016/j.jobe.2022.104081.
443 [17] J.C. Morel, A. Mesbah, M. Oggero, P. Walker, Building houses with local
444 materials: Means to drastically reduce the environmental impact of construction,
445 Build. Environ. 36 (2001) 1119–1126. doi:10.1016/S0360-1323(00)00054-8.
446 [18] D. Allinson, M. Hall, Hygrothermal analysis of a stabilised rammed earth test
447 building in the UK, Energy Build. 42 (2010) 845–852.
448 doi:10.1016/j.enbuild.2009.12.005.
449 [19] C.T.S. Beckett, R. Cardell-Oliver, D. Ciancio, C. Huebnerc, Measured and
450 simulated thermal behaviour in rammed earth houses in a hot-arid climate. Part
451 B: Comfort, J. Build. Eng. 13 (2017) 146–158.
452 doi:https://doi.org/10.1016/j.jobe.2017.07.013.
453 [20] C.T.S. Beckett, R. Cardell-Oliver, D. Ciancio, C. Huebnerc, Measured and
454 simulated thermal behaviour in rammed earth houses in a hot-arid climate. Part
455 A: Structural behaviour, J. Build. Eng. 15 (2018) 243–251.
456 doi:https://doi.org/10.1016/j.jobe.2017.11.013.
457 [21] Q.B. Bui, J.C. Morel, B. V. Venkatarama Reddy, W. Ghayad, Durability of
458 rammed earth walls exposed for 20 years to natural weathering, Build. Environ.
459 44 (2009) 912–919. doi:10.1016/j.buildenv.2008.07.001.
460 [22] S. Ghasemalizadeh, V. Toufigh, Durability of Rammed Earth Materials, Int. J.
461 Geomech. 20 (2020) 04020201. doi:10.1061/(asce)gm.1943-5622.0001829.
462 [23] V. Toufigh, E. Kianfar, The effects of stabilizers on the thermal and the
463 mechanical properties of rammed earth at various humidities and their
464 environmental impacts, Constr. Build. Mater. 200 (2019) 616–629.
465 doi:10.1016/j.conbuildmat.2018.12.050.

[24] Q.B. Bui, J.C. Morel, S. Hans, P. Walker, Effect of moisture content on the mechanical characteristics of rammed earth, Constr. Build. Mater. 54 (2014) 163–169. doi:10.1016/j.conbuildmat.2013.12.067.

[25] V. Maniatidis, P. Walker, Structural Capacity of Rammed Earth in Compression, J. Mater. Civ. Eng. 20 (2008) 230–238. doi:10.1061/(asce)0899-1561(2008)20:3(230).

[26] G. Lan, S. Chao, Y. Wang, K. Zhang, Study of compressive strength test methods for earth block masonry—Capping method and loading mode, J. Build. Eng. 43 (2021) 103094. doi:https://doi.org/10.1016/j.jobe.2021.103094.

[27] T.T. Bui, Q.B. Bui, A. Limam, S. Maximilien, Failure of rammed earth walls: From observations to quantifications, Constr. Build. Mater. 51 (2014) 295–302. doi:10.1016/j.conbuildmat.2013.10.053.

[28] T.T. Bui, Q.B. Bui, A. Limam, J.C. Morel, Modeling rammed earth wall using discrete element method, Contin. Mech. Thermodyn. 28 (2016) 523–538. doi:10.1007/s00161-015-0460-3.

[29] R. El-Nabouch, Q.B. Bui, O. Plé, P. Perrotin, Assessing the in-plane seismic performance of rammed earth walls by using horizontal loading tests, Eng. Struct. 145 (2017) 153–161. doi:10.1016/j.engstruct.2017.05.027.

[30] L. Miccoli, U. Müller, P. Fontana, Mechanical behaviour of earthen materials: A comparison between earth block masonry, rammed earth and cob, Constr. Build. Mater. 61 (2014) 327–339. doi:10.1016/j.conbuildmat.2014.03.009.

[31] Q.B. Bui, T.T. Bui, R. El-Nabouch, D.K. Thai, Vertical Rods as a Seismic Reinforcement Technique for Rammed Earth Walls: An Assessment, Adv. Civ. Eng. 2019 (2019). doi:10.1155/2019/1285937.

[32] R.A. Silva, D. V. Oliveira, L. Schueremans, P.B. Lourenço, T. Miranda,

491 Modelling the structural behaviour of rammed earth components, Civil-Comp
492 Proc. 106 (2014). doi:10.4203/ccp.106.112.
493 [33] M. Hall, D. Allinson, Assessing the effects of soil grading on the moisture
494 content-dependent thermal conductivity of stabilised rammed earth materials,
495 Appl. Therm. Eng. 29 (2009) 740–747.
496 doi:10.1016/j.applthermaleng.2008.03.051.
497 [34] S. Samadianfard, V. Toufigh, Energy Use and Thermal Performance of Rammed-
498 Earth Materials, J. Mater. Civ. Eng. 32 (2020) 04020276.
499 doi:10.1061/(asce)mt.1943-5533.0003364.
500 [35] J. Tinsley, S. Pavía, Thermal performance and fitness of glacial till for rammed
501 earth construction, J. Build. Eng. 24 (2019) 100727.
502 doi:https://doi.org/10.1016/j.jobe.2019.02.019.
503 [36] P.A. Chabriac, A. Fabbri, J.C. Morel, J.P. Laurent, J. Blanc-Gonnet, A procedure
504 to measure the in-situ hygrothermal behavior of earth walls, Materials (Basel). 7
505 (2014) 3002–3020. doi:10.3390/ma7043002.
506 [37] A. Niampira Daza, E. Zambrano, J. Alcides Ruiz, Acoustic performance in raw
507 earth construction techniques used in Colombia, in: EuroRegio2016, Porto,
508 Portugal, 2016.
509 [38] Q.B. Bui, J.C. Morel, The creep of Rammed Earth material, in: Rammed Earth
510 Constr. - Proc. 1st Int. Conf. Rammed Earth Constr. ICREC 2015, 2015: pp. 51–
511 56. doi:10.1201/b18046-11.
512 [39] H.N. Abhilash, J.-C. Morel, Stress–Strain Characteristics of Unstabilised
513 Rammed Earth, in: B. V. V. Reddy et al. (Ed.), Earthen Dwellings Struct.,
514 Springer Nature, 2019: pp. 203–214. doi:10.1007/978-981-13-5883-8_18.
515 [40] EN_ISO_17892-4:2019, Geotechnical investigation and testing - Laboratory

testing of soil - Part 4: Determination of particle size distribution, 2016.

[41] J.E. Aubert, A. Marcom, P. Oliva, P. Segui, Chequered earth construction in south-western France, J. Cult. Herit. 16 (2015) 293–298. doi:10.1016/j.culher.2014.07.002.

[42] M.I. Gomes, T.D. Gonçalves, P. Faria, Unstabilized rammed earth: characterization of material collected from old constructions in south Portugal and comparison to normative requirements, Int. J. Archit. Herit. 8 (2014) 185–212. doi:https://doi.org/10.1080/15583058.2012.683133.

[43] P. Walker, R. Keable, J. Martin, V. Maniatidis, Rammed earth: design and construction guidelines, (2005).

[44] H. Houben, H. Guillaud, CRAterre. Earth construction : a comprehensive guide, London: Intermediate Technology Publications, 1994.

[45] J.E. Aubert, A. Fabbri, J.C. Morel, P. Maillard, An earth block with a compressive strength higher than 45 MPa!, Constr. Build. Mater. 47 (2013) 366–369. doi:10.1016/j.conbuildmat.2013.05.068.

[46] J. Canivell, J.J. Martín-del-Río, R.M. Falcón, C. Rubio-Bellido, Rammed earth construction: A proposal for a statistical quality control in the execution process, Sustain. 12 (2020). doi:10.3390/su12072830.

[47] EN 12390-1, Testing hardened concrete. Part 1: Shape, dimensions and other requirements for specimens and moulds, Brussels, Belgium: Comité Européen de Normalisation, 2013.

[48] A. Arrigoni, R. Pelosato, G. Dotelli, C.T.S. Beckett, D. Ciancio, Weathering's beneficial effect on waste-stabilised rammed earth: a chemical and microstructural investigation, Constr. Build. Mater. 140 (2017) 157–166. doi:10.1016/j.conbuildmat.2017.02.009.

[49] D. Alós Shepherd, E. Kotan, F. Dehn, Plastic concrete for cut-off walls: A review, Constr. Build. Mater. 255 (2020). doi:10.1016/j.conbuildmat.2020.119248.

[50] CEN, Eurocode 2: Design of concrete structures - Part 1–1: General rules and rules for buildings UNE-EN 1992-1-1, European Committee for Standardization. Brussels, 2004.

[51] A.E.N.D.C., First Report on Viscosity and Plasticity, Nature. 136 (1935) 697–699. doi:10.1038/136697a0.

[52] W. Flugge, Viscoelasticity, Blaisdell Publishing Co., New York, 1967.

[53] G.S. Blair, The role of psychophysics in rheology, J. Colloid Sci. 2 (1947) 21–32. doi:10.1016/0095-8522(47)90007-X.

[54] X. Ni, S. Cao, Y. Li, S. Liang, Stiffness degradation of shear walls under cyclic loading: experimental study and modelling, Springer Netherlands, 2019. doi:10.1007/s10518-019-00682-5.

[55] T. Keller, T. Tirelli, A. Zhou, Tensile fatigue performance of pultruded glass fiber reinforced polymer profiles, Compos. Struct. 68 (2005) 235–245. doi:10.1016/j.compstruct.2004.03.021.

[56] J. Lee, G.L. Fenves, A plastic-damage concrete model for earthquake analysis of dams, Earthq. Eng. Struct. Dyn. 27 (1998) 937–956. doi:10.1002/(SICI)1096-9845(199809)27:9<937::AID-EQE764>3.0.CO;2-5.